†Research sponsored by the U. S. Air Force Office of Scientific Research, Office of Aerospace Research under AFOSR Grant No. 68-1494A.

*Present address: University of East Anglia, Norwich, England.

[1]P. K. Larsen and K. Saermark, Phys. Letters 24A, 374 (1967); 24A, 668 (1967); 26A, 296 (1968).

[2]J. R. Houck, H. V. Bohm, B. W. Maxfield, and J. W. Wilkins, Phys. Rev. Letters 19, 224 (1967).

[3]A. G. Betjemann, H. V. Bohm, D. J. Meredith, and E. R. Dobbs, Phys. Letters 25A, 753 (1967).

[4]R. L. Thomas, G. Turner, and H. V. Bohm, Phys. Rev. Letters 20, 207 (1968).

[5]B. Abeles, Phys. Rev. Letters 19, 1181 (1967).

[6]D. J. Meredith, R. J. Watts-Tobin, and E. R. Dobbs, J. Acoust. Soc. Am. 45, 1393 (1969).

[7]M. R. Gaerttner, W. D. Wallace, and B. W. Maxfield, Phys. Rev. 184, 702 (1969).

[8]V. F. Gantmakher and V. T. Dolgopolov, Zh. Eksperim. i Teor. Fiz. 57, 132 (1969) [Sov. Phys. JETP 30, 78 (1970)].

[9]W. D. Wallace, M. R. Gaerttner, and B. W. Maxfield, Bull. Am. Phys. Soc. 14, 64 (1969).

[10]R. L. Thomas, G. Turner, and D. Hsu, Phys. Letters 30A, 316 (1969).

[11]J. J. Quinn, Phys. Letters 25A, 522 (1967).

[12]For a recent bibliography of this subject, see, for example, R. L. Thomas and G. Turner, Phys. Rev. 176, 768 (1968).

[13]R. L. Thomas and R. V. Bohm, Phys. Rev. Letters 16, 587 (1966).

[14]T. Kjeldaas, Phys. Rev. 113, 1473 (1959).

[15]R. Casànova Alig, Phys. Rev. 178, 1050 (1969).

[16]P. D. Southgate, J. Appl. Phys. 40, 22 (1969).

[17]Equation (5) differs only in a phase factor $\pm i$ which is absent in the equivalent result of Quinn (Ref. 11).

[18]The difference in attenuation leads to the resultant also being slightly elliptically polarized.

[19]A. B. Pippard, Proc. Roy. Soc. (London) A257, 165 (1960).

[20]N. Tepley, Proc. IEEE 53, 1586 (1965).

[21]G. H. Kamm and H. V. Bohm, Rev. Sci. Instr. 33, 957 (1962).

[22]The minimum rather than maximum was investigated simply to allow full use of instrumental sensitivity.

[23]P. A. Penz and T. Kushida, Phys. Rev. 176, 804 (1968).

[24]In fact, the implied boundary conditions required in the infinite medium approximation prevent direct application of the theory of Sec. II. We take the view that the complications involved here are unlikely to be important physically. Also, note that this result is the same as Eq. (5) in R. C. Alig, J. J. Quinn, and S. Rodriguez, Phys. Rev. 148, 632 (1966).

[25]E. R. Dobbs, R. L. Thomas, and D. Hsu, Phys. Letters 30A, 338 (1969); E. R. Dobbs, J. Phys. Chem. Solids 31, 1657 (1970).

PHYSICAL REVIEW B VOLUME 3, NUMBER 10 15 MAY 1971

de Haas-van Alphen Effect in Mercury†

R. G. Poulsen,* J. S. Moss,‡ and W. R. Datars§

Department of Physics, McMaster University, Hamilton, Ontario

(Received 2 October 1970)

We report the results of a detailed investigation of the de Haas–van Alphen effect in single-crystal mercury. The data were taken for the three major crystallographic planes in magnetic fields extending up to 116 kG and at a temperature of 1.2 °K. The frequencies have been assigned to orbits on the second-band electron-lens surface and on the first-band hole surface. Several new extremal orbits on the first-band surface are reported. The results are in general accord with the Fermi surface deduced from other experiments and from band-structure calculations.

I. INTRODUCTION

There have been several recent studies of the Fermi surface of crystalline mercury. However, there is a need to complete de Haas–van Alphen (dHvA) frequency measurements to a uniform accuracy. This work reports the results of an extensive dHvA experiment to provide more accurate and complete dHvA frequency measurements and to extend the understanding of the Fermi surface of rhombohedral mercury.

Previous dHvA experiments in mercury were carried out by Verkin, Lazarev, and Rudenko,[1] Shoenberg,[2] and Brandt and Rayne.[3] The work of Brandt and Rayne, which was the most extensive of the three, gave dHvA frequencies of several extremal orbits in principal crystallographic planes and the general topology of the Fermi surface of mercury. Other reported work on the Fermi surface of mercury includes cyclotron resonance experiments by Dixon and Datars,[4] magnetoresistance experiments by Datars and Dixon[5] and Dishman and Rayne,[6] and magnetoacoustic experiments by Bogle *et al.*[7] These experimental results are in essential agreement with the Fermi-surface topologies determined from the relativistic-augmented-plane-wave (RAPW) model of Keeton and Loucks,[8] the empirical MAGV model of Dishman and Rayne,[6]

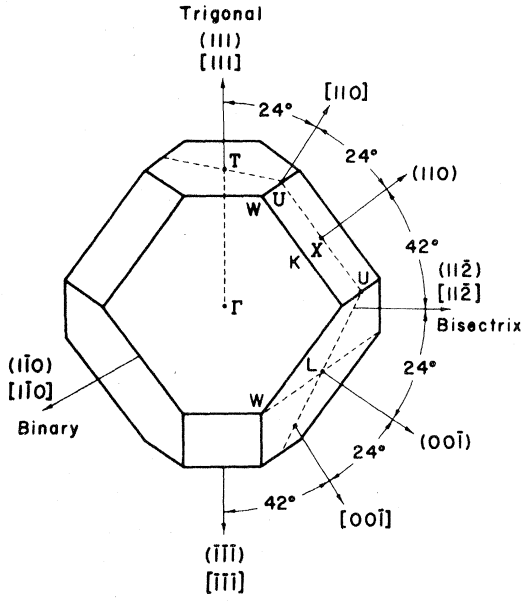

FIG. 1. The Brillouin zone for mercury showing some directions (lmn) in reciprocal space and $[lmn]$ in real space.

and a variety of pseudopotential models.[3,6,7] However, none of these models can simultaneously and accurately describe the hole surface, the electron surface, and the magnetoresistance data. The present work is discussed in terms of these models for the Fermi surface and provides information about additional extremal cross sections of the Fermi surface.

II. FERMI SURFACE OF MERCURY

The first Brillouin zone[8,9] of rhombohedral mercury with symmetry points and principal symmetry axes labeled in accord with previous work on mercury is shown in Fig. 1. The Fermi surface of mercury, which has a volume equal to that of the Brillouin zone, cuts through the L faces to yield lens-shaped second-zone electron surfaces centered at L on the (100) faces of the Brillouin zone, and a multiply connected first-zone hole surface. Unlike the free-electron sphere, however, the actual Fermi surface[3-8] also appears to contact the X and T faces to produce openings in the hole surface centered at X and T. A nearly free-electron model[4,5] of the first-zone Fermi surface of mercury viewed from the [111] direction is shown in Fig. 2 with markings to illustrate breakthrough at X and T and some extremal orbits. The outsides of the solid lines near X and T represent the breakthrough-region sizes predicted by Keeton and Loucks[8] while the dotted lines represent those predicted by the MAG V model of Dishman and Rayne.[6] Black areas on the model are regions where the surface is joined to other parts of the extended-zone surface.[4,5] In the actual hole surface, the sharp corners are expected to be more round, and the X-face section is expected to be narrower.

In what follows, the pair of arms on either side of the breakthrough region near the X face in Fig. 2 will be called the "β arms," and the breakthrough regions at L, X, and T will be called the L, X, and T face openings, respectively. We adopt the notation that (lmn) represents a direction in reciprocal space, or a plane perpendicular to the (lmn) direction. Real-space directions are represented by $[lmn]$. Sets of equivalent directions will be represented by $\{lmn\}$ in reciprocal space and by $\langle lmn\rangle$ in real space.

Observation of the $\mu\gamma$ and γ_2 orbits shown in Fig. 2 are reported for the first time in this study. These orbits, and the κ and ν orbits, have limited range. The $\mu\gamma$ orbit is expected to exist for an angular range of magnetic field direction of about $\pm 6°$ centered approximately 13° from the (11$\bar{2}$) direction in the (111) plane, with its minimum dHvA frequency about 30° from this center toward (110). The γ_2 orbit is expected to be observed only in or very near the (1$\bar{1}$0) plane from a sharp cutoff near the (11$\bar{2}$) direction toward the (110) direction; the position of this cutoff depends sensitively on the size of the T-face opening and on the β-arm shape near K. The κ orbit cannot occur

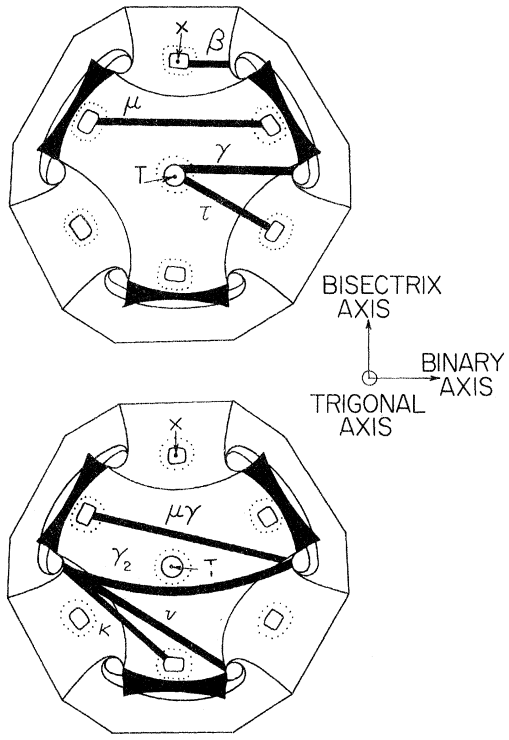

FIG. 2. Some possible hole orbits on the first-zone Fermi surface of mercury shown on a nearly free-electron model viewed along the trigonal (111) direction.

for field directions in either of the $(1\bar{1}0)$ or $(11\bar{2})$ planes, but is expected to occur for a very limited range of $(15 \pm 3)^\circ$ from the $(11\bar{2})$ direction in the (111) plane. Finally, the ν orbit is expected to have a range of approximately $\pm 3^\circ$ centered at the $(1\bar{1}0)$ direction in the (111) plane, which depends entirely on the β-arm shape near K. The hole surface also supports a large hexagonal-shaped orbit η around the outside of the T face for field directions near the (111) direction.

The electron lenses support α orbits which exist for all field directions. For the lens normal to (100), for example, the α-orbit dHvA frequencies are largest with $\vec{H}$ near the (100) direction and smallest for $\vec{H}$ near the (100) plane.

III. EXPERIMENTAL METHOD

Both the field modulation and torque methods were used in measuring the dHvA effect. The torque magnetometer, described earlier by Vanderkooy and Datars,[10] was used for aligning some of the crystals in the field of a 20-kG rotatable iron magnet. The large-amplitude field modulation magnetometer of conventional design[11,12] was used with the fields of 57- and 116-kG superconducting solenoids. All data were taken at 1.2 °K.

A modulation frequency of 517 Hz was used and the modulation amplitude was limited to less than 75 G, above which the magnet was driven normal. This frequency was chosen to give the best signal-to-noise ratio for the dominant γ and τ signals. At this frequency there was complete penetration of the mercury sample because the large magnetoresistance made the skin depth large. The pickup coils were impedance matched to a twin-T filter to remove the fundamental frequency ω and the signals were phase sensitively detected at harmonics $n\omega$ with a PAR HR-8 lock-in amplifier. Harmonics from the second to the seventh were used, low harmonics to obtain a general view of the dHvA spectra, and the seventh to enhance low-amplitude high-dHvA-frequency signals relative to strong low-frequency signals. For the higher harmonics, the skin depth may not have been greater than the sample dimensions. While such conditions could have decreased signal amplitude, they would not have caused errors in the dHvA frequencies which were measured in this work. Optional-band-pass filters tuned to the harmonic of interest were used occasionally between the twin-T and lock-in amplifier. The output from the PAR was filtered by a Krohn-Hite 3322R band-pass filter principally to remove background drift. The filtered signals were recorded on magnetic tape together with magnetic field voltages using a data acquisition system for subsequent Fourier analysis. Usually the field was scanned[13] linearly in $1/H$, and typically 10 to 20 pairs of field and dHvA voltages were recorded per dHvA oscillation for over 100 oscillations. For the Fourier analysis, the data were first presmoothed by subtracting a least-squares parabola fitted to the data and then interpolating for signal values spaced equally in reciprocal field. It was found necessary to presmooth the field values locally for traces in which many points were recorded to ensure a monotonic data table. A fast Fourier-transform computer subroutine was then used to compute the Fourier amplitude for the dHvA frequency range of interest. The square root of the Fourier amplitude vs dHvA frequency was generally plotted on a Benson-Lehner plotter. Taking the square root resulted in suppressed dominant peaks and improved visibility of low-amplitude peaks.

A sample Fourier-amplitude and dHvA frequency plot is shown in Fig. 3. The Fourier-amplitude plot corresponds to an experimental trace with $\vec{H}$ along the $(11\bar{2})$ direction detected by the seventh harmonic to suppress signals of the γ branch. The frequency plot shows the variety of harmonic and sum frequencies observed and demonstrates the need for Fourier analysis in resolving the spectra. The γ_2 frequency branch, which is first reported in this work, is seen to correspond to a relatively strong signal in the Fourier-amplitude plot.

The large number of harmonic and sum frequencies in Fig. 3 may be evidence of magnetic interaction effects such as those observed by Phillips and Gold[14] while the difference frequencies are probably absent because the modulation amplitude was chosen so that the seventh-order Bessel function would reduce the amplitudes of the lower-frequency dHvA signals. However, no detailed attempt was made to determine the origin of the harmonic and combinational frequencies and these will be ignored in subsequent discussion.

Small mercury samples were grown, from 99.9999% pure mercury supplied by the United Mineral Corporation of New York, with a modified Bridgeman technique similar to that described by Dixon and Datars.[4] Initially, measurements could only be made to within about 5° of major crystallographic planes because of difficulties in accurately orienting the small samples by back-reflection Laue techniques and then mounting them in the dHvA apparatus in liquid nitrogen. Consequently, samples were grown inside a very small goniometer designed to fit accurately inside the rotatable cylindrical sample holder of the dHvA apparatus. Measurements could then be made within $\pm 1^\circ$ of desired crystal planes after first adjusting the goniometer in a series of torque magnetometer experiments. A combination of β-arm dHvA oscillations and induced-torque open-orbit peaks[15] were used to determine corrections to the goniometer adjustment. For example, with the torque magne-

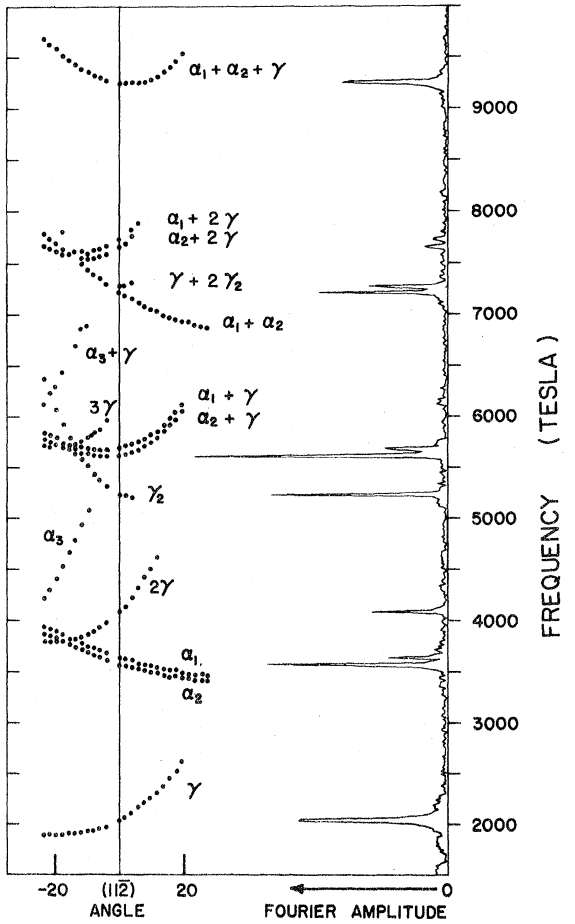

FIG. 3. Sample Fourier-amplitude plot at the (11$\bar{2}$) direction and dHvA frequency plot in the region of the (11$\bar{2}$) direction for fields in the (1$\bar{1}$0) plane.

tometer and goniometer axes both vertical, the goniometer was adjusted so that the dHvA frequencies from the three β-arm branches were similar as nearly as possible, in order to orient a sample for measurements in the binary-bisectrix (111) plane. Similarly, for measurements in the trigonal-bisectrix (1$\bar{1}$0) plane, the goniometer was adjusted so that the beating dHvA frequencies from the [100] and [010] β arms were equal, while the open-orbit peaks corresponding to the (100), (010), and (110) open-orbit directions coalesced into one at [001]. Accurate goniometer adjustments were possible for these cases since the features described are all very sensitive to crystal orientation.

IV. EXPERIMENTAL RESULTS AND DISCUSSION

A. Trigonal-Bisectrix Plane

Figures 4 and 5 show the dHvA frequency plots for a sample oriented in the trigonal-bisectrix (1$\bar{1}$0) plane. The data in Fig. 4 agree closely with the solid curve based on a fourth-order fit to β-arm quantum oscillations on the microwave surface impedance.[16]

The γ branch in Fig. 5 is assigned to the γ orbit from the position of the minimum and its angular range. This was originally assigned to the τ orbit by Brandt and Rayne.[3] The minimum frequency is (1900 ± 10) T, 19° from the (11$\bar{2}$) direction toward the (110) direction, and the frequencies at (110) and (11$\bar{2}$) directions are (2080 ± 10) and (2040 ± 10) T, respectively.

The γ_2 branch is assigned to the γ_2 orbit illustrated in Fig. 2 because of the cutoff near the (11$\bar{2}$) direction and the increase in frequency toward the (110) direction. The cutoff depends critically on the size of the T-face opening and on the amount by which the β arms pass inside the X face at K. Assuming that the orbit passes through K, the radius of the T-face opening would be approximately 0.2 Å^{-1}, which is in agreement with the value of 0.198 Å^{-1} estimated by Dishman and Rayne[6] from the MAG V model. There may be evidence of the γ_2 orbit in the experiment of Bogle *et al.*[7] The break in the points labeled γ in Fig. 2 of Ref. 7 may indicate that not only γ but also γ_2 orbits were observed because for $\vec{H}$ near the (11$\bar{2}$) direction, the Fermi-surface calipers along the (111) direction of the γ and γ_2 orbits are approximately equal.

The frequency branch η was observed only with the 116-kG magnet. This branch is assigned to the hexagonal-shaped hole orbit η centered at T and completely enclosing the T face. The orbit has a minimum frequency of 21 900 T at the (111) direction with an angular extent of 12° toward the (100) direction, where it is cut off sharply by the L-face opening, and 18.4° toward the (110) direction where it is cut off sharply by the X-face opening. Bogle *et al.*[7] predict similar angular ranges and report a caliper dimension $k_{TW}^{\text{out}} \sim 0.90$ Å^{-1} from T through W to the outside of the hole surface. The frequency corresponding to a hexagon with this dimension is 22 100 T and compares favorably with the minimum value of 21 900 T observed in this experiment.

The dHvA frequency region between 50 and 5000 was carefully studied about the (1$\bar{1}$0) and (111) directions for the X-face and T-face electron necks. A frequency of 1950 T, which may be that of the T-face electron neck orbit, was observed along the (111) direction in one crystal. However, this assignment is tentative because the frequency was not observed in other samples with the same orientation. The X-face neck was not observed, perhaps because the electron bands are very narrow or because the oscillations are sensitive to strain-induced phase smearing. The μ orbit, which has been observed by the magnetoacoustic effect,[7] has not been observed by dHvA.

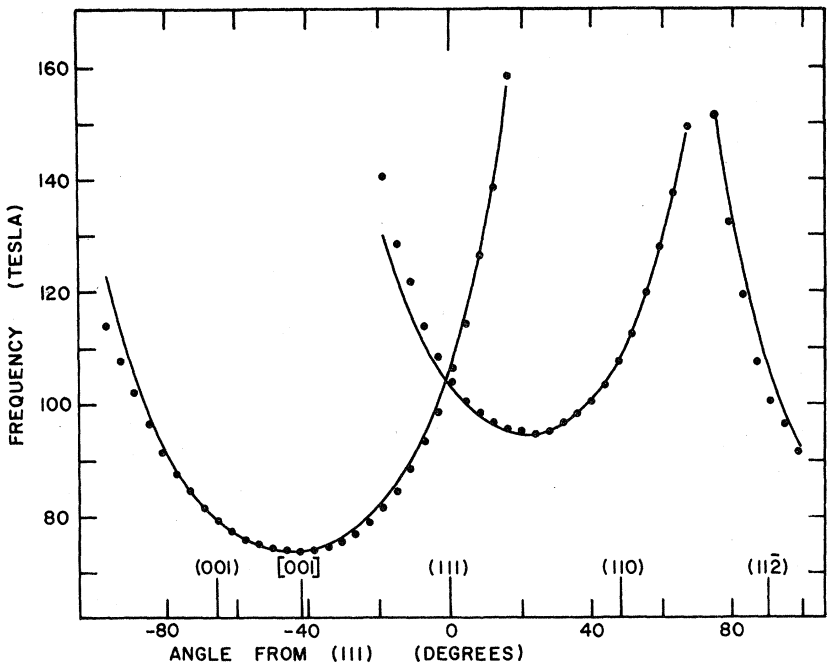

FIG. 4. β-arm dHvA frequencies for the $(1\bar{1}0)$ plane. The solid curve was calculated from results of a fourth-order fit to frequencies of β-arm quantum oscillations.

It is possible that the μ orbit is obscured by the variety of signals near the $(11\bar{2})$ direction in Fig. 3 or that it has a low spin-splitting factor for dHvA measurement.

Because curves α_1 and α_2 extend through 180°, they are assigned to α orbits on the electron lenses normal to (100) and (010) directions. These two branches are resolved by an amount that indicates that the crystal was rotated about 1° out of the trigonal-bisectrix plane about an axis at approximately the −40° position in Fig. 5. The α_3 branch with a minimum frequency of 3250 T is assigned to an α orbit on the electron lens normal to the (001) axis. The amplitudes of the signals corresponding to the α branches all decreased rapidly with increasing dHvA frequency, and α_3 did not reappear near the (001) direction at higher frequencies, even at 100 kG. The 6800-T α frequency reported by Brandt and Rayne[3] is a sum frequency $\alpha+\gamma$; at the (001) direction α_3 is expected to be greater than 9500 T since $k_{LU}=0.538$ Å^{-1} for the electron lens.[7]

Spin-splitting zeros may also have contributed to the rapid decrease in amplitude of the α-orbit signals, since for $0.61<m_t^*<1.8$ and $g\gtrsim 2$, the spin-splitting factor $\cos(\frac{1}{2}\pi g m_t^*)$ will go through one or more zeros. Little can be said about this effect, however, because the signals did not reappear at high frequencies; attempts, based on an ellipsoidal model for the electron lens, to use the dHvA amplitude terms to determine effective g values $(2n+1)/m_t^*$ were inconclusive.

B. Binary-Bisectrix Plane

dHvA frequency plots for a sample oriented near the binary-bisectrix (111) plane are shown in Figs. 6 and 7. The 7-T spread of the minimum β frequencies in Fig. 6 indicates that the sample is oriented within 1.4° of the (111) plane since in Fig. 4 the β frequency varies 2.6 T/deg for the low-frequency branch where $\vec{H}$ is 90° from the (111)

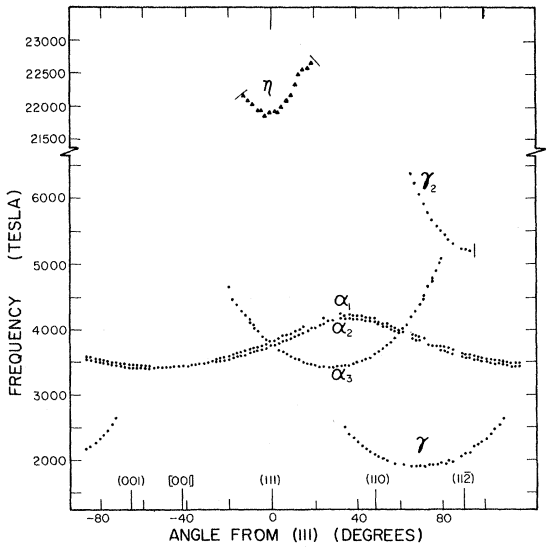

FIG. 5. The dHvA frequencies greater than 1500 T for the $(1\bar{1}0)$ plane.

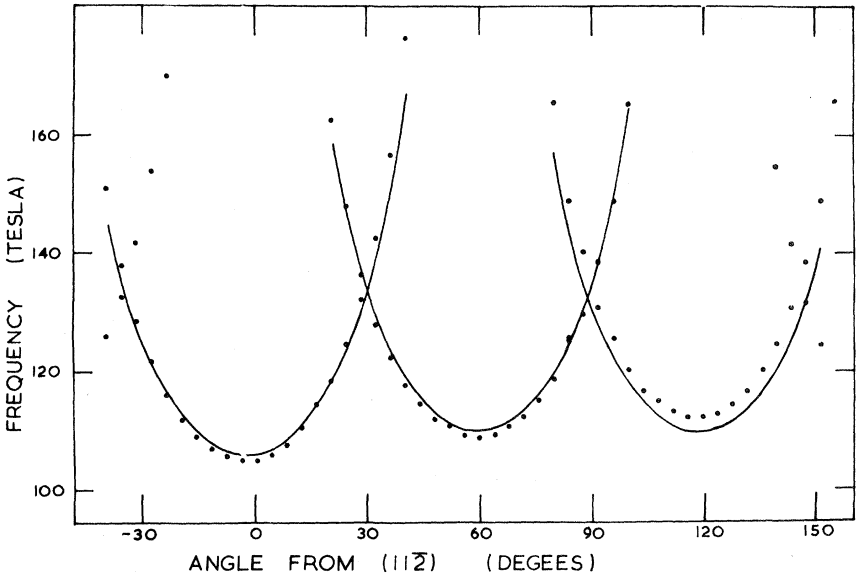

FIG. 6. β-arm dHvA frequencies for the (111) plane. The solid curve was calculated from results of a fourth-order fit to frequencies of β-arm quantum oscillations.

direction. The solid lines in Fig. 6 are the best least-squares fit of the data to a β-frequency model to be discussed elsewhere.[16]

In Fig. 7, the α-frequency branches arise from α orbits on the electron lenses, and the γ and τ branches are assigned to γ and τ orbits since their minima are at (11$\bar{2}$) and (1$\bar{1}$0) directions as expected. The minimum frequencies for α and τ are 3240 and 1570 T, respectively, at the (1$\bar{1}$0) direction while the minimum frequency for γ is 2060 T at the (11$\bar{2}$) direction.

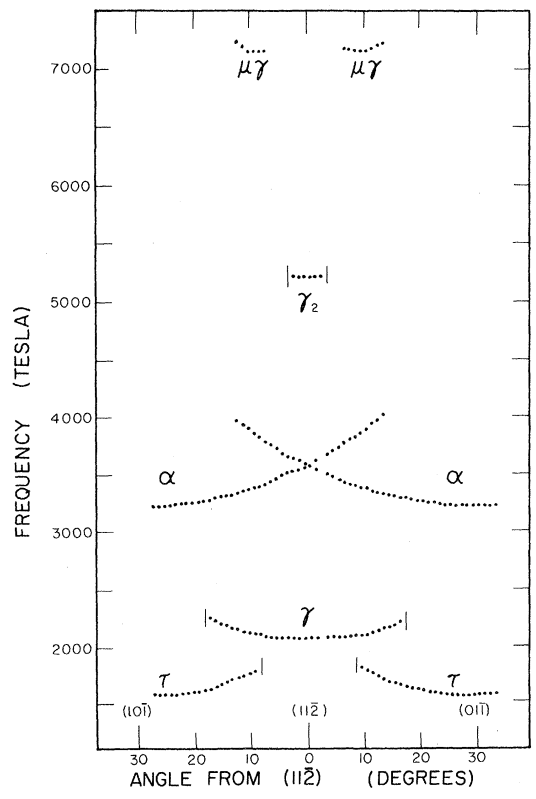

FIG. 7. The dHvA frequencies greater than 1500 T for the (111) plane of mercury.

The γ_2 branch in Fig. 7 is assigned to the γ_2 orbit because its frequency of 5200 T corresponds to that for the γ_2 branch near the (11$\bar{2}$) direction in Fig. 5. The assignment of both these branches to the γ_2 orbit is confirmed by the sudden cutoffs of this γ_2 branch, just 2.5° to either side of the (11$\bar{2}$) direction in Fig. 7, as expected for the γ_2 orbit. The $\mu\gamma$ branches in Fig. 7 are assigned to the $\mu\gamma$ orbit, since they were observed over angular ranges for which this orbit is most probable in Fig. 2. It is not certain, however, that these branches may not correspond to the κ orbit which has a range of about 12° to 18° from the (11$\bar{2}$) direction toward the (1$\bar{1}$0) direction.

The angular range of 41.2° of the τ branch in Fig. 7 means that the sum $k^{\text{in}}_{TW}+k^{\text{in}}_{XK}$ is at least, but perhaps greater than, 0.39_5 Å^{-1}. The k^{in}_{TW} is the inside dimension of the T-face opening of the hole surface along TW while k^{in}_{XK} is the inside dimension of the X-face opening along the XK line. This value is essentially the same as the value of 0.40_7 obtained from the MAG V model,[6] but nearly twice that obtained from the RAPW model[8] which is seen to underestimate the sizes of the X- and T-face openings. The present results yield a minimum value for $k^{\text{in}}_{TW}+k^{\text{in}}_{XK}$ whereas the magnetoresistance results, summarized in the MAG V model, yield a maximum value for this dimension. Taken together these measurements show that the sum $k^{\text{in}}_{TW}+k^{\text{in}}_{XK}$ is 0.40 Å^{-1}. Also the sharp cutoffs of

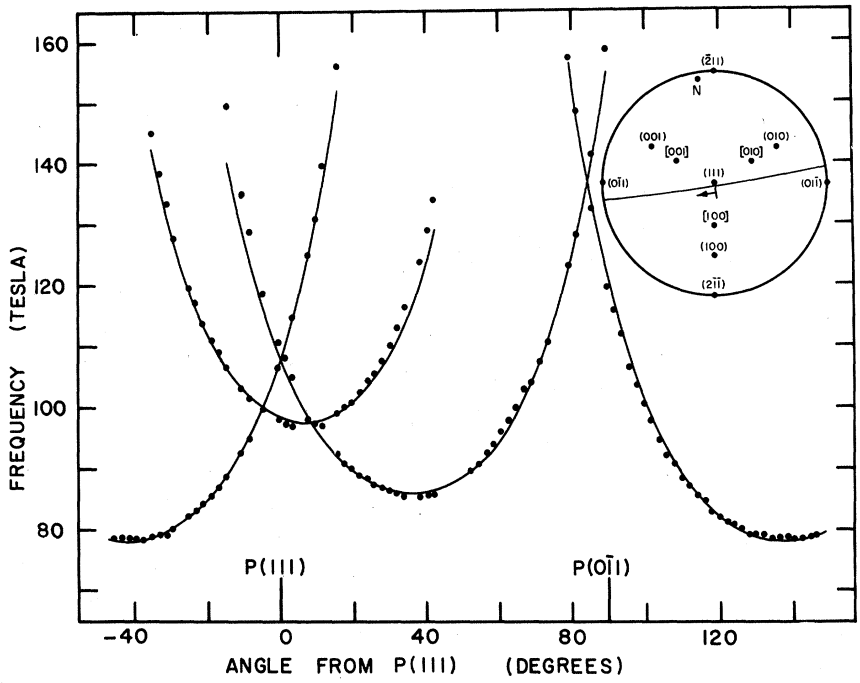

FIG. 8. β-arm dHvA frequencies for a plane near the ($\bar{2}$11) plane of mercury. The solid line in the stereogram shows the orientation of the measured plane: The normal N has coordinates (86.5, 9.0). P(111) and P(0$\bar{1}$1) show the projection of directions (111) and (0$\bar{1}$1) on the plane of measurement. The solid curve was calculated from results of a fourth-order fit to frequencies of β-arm quantum oscillations.

the γ_2 branch 2.5° to either side of the (11$\bar{2}$) direction in Fig. 7 mean that 0.866 $k_{XK}^{\text{out}} + k_{TU}^{\text{in}} \lesssim 0.47$, where k_{XK}^{out} is the distance from X through K to the outside of the β arm near K. The amplitudes did not drop suddenly near the ends of the γ branch in Fig. 7, thus indicating that this branch was not observed over the total angular range for which the γ orbit is geometrically possible. However, the angular range of 33.5° over which γ was observed means that 0.866 $k_{XK}^{\text{out}} - k_{TU}^{\text{in}}$ must be less than 0.18 Å^{-1}. Thus, the measured angular ranges of the τ, γ_2, and γ orbits show that $k_{XK}^{\text{out}} \lesssim 0.38$ Å^{-1}, $k_{TU}^{\text{in}} > 0.15$ Å^{-1}, and $k_{XK}^{\text{in}} < 0.25$ Å^{-1}, where the inequalities arise primarily from the uncertainty in the angular range of the γ branch.

C. Trigonal-Binary Plane

The dHvA frequency plots for a sample oriented near the trigonal-binary ($\bar{2}$11) plane are shown in Figs. 8 and 9. The sample was not oriented with

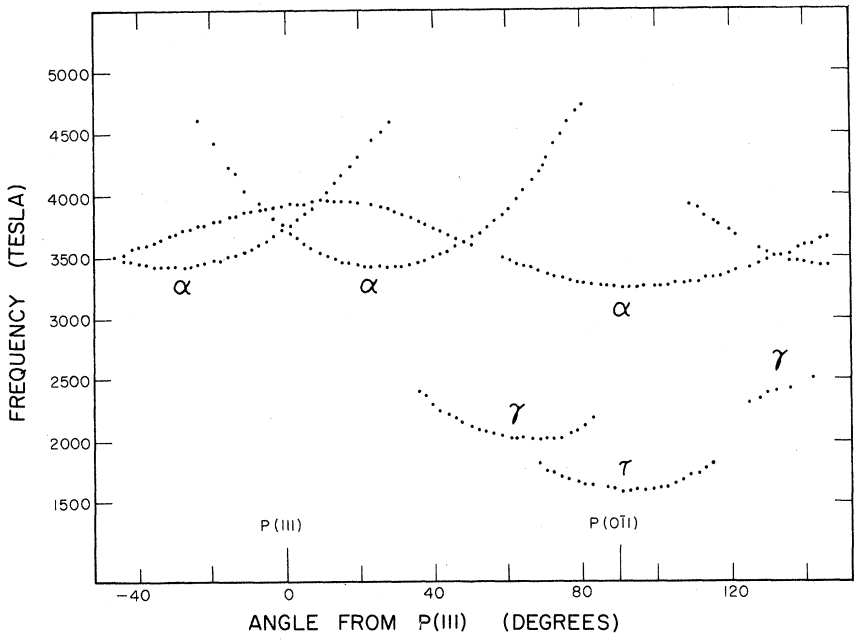

FIG. 9. The dHvA frequencies greater than 1500 T for a plane near the ($\bar{2}$11) plane as specified in the stereogram in Fig. 8.

TABLE I. Some dHvA frequencies and extremal cross-section areas of mercury.

Orbit	Field direction (deg)		dHvA frequency (T)	Area (in a.u.)
β	2 from toward	(001) (001) [a]	73.9 ± 0.5	1.98×10^{-3}
γ	19 from toward	(11$\bar{2}$) (110) [a]	1900 ± 10	5.08×10^{-2}
		(110)	2080 ± 10	5.56×10^{-2}
		(11$\bar{2}$)	2060 ± 10	5.50×10^{-2}
τ		(0$\bar{1}$1) [a]	1570 ± 10	4.19×10^{-2}
η		(111) [a]	21 900 ± 300	5.85×10^{-1}
T neck		(111)	1950	5.21×10^{-2}
α [b]		(111)	3780 ± 10	1.01×10^{-1}
		(110)	3410 ± 10	9.11×10^{-2}
		(110)	3630 ± 10	9.70×10^{-2}
		(1$\bar{1}$0) [a]	3240 ± 10	8.89×10^{-2}
		(11$\bar{2}$)	3580 ± 10	9.56×10^{-2}
γ_2		(11$\bar{2}$)	5200 ± 10	13.9×10^{-2}
$\mu\gamma$	8 from toward	(11$\bar{2}$) (1$\bar{1}$0)	7150 ± 10	19.1×10^{-2}

[a]Directions of minimum dHvA frequency for the orbit.
[b]The α-orbit values correspond to the lens normal to (001).

the goniometer used for the other planes. The actual orientation was obtained with a computer program in which a search was made for the orientation yielding the best least-squares fit of the measured β-arm frequencies to the β-arm dHvA frequency model, which will be discussed elsewhere.[16] The best fit and the orientation corresponding to it are shown in Fig. 8; the normal N to the measured plane has angular coordinates (86.5, 9.0) in the stereographic projection.

The frequency branches α in Fig. 9 are from the α orbits on the electron lenses. The branch τ has been assigned to a τ orbit since its minimum is near the projection of the (0$\bar{1}$1) direction on the plane of measurement. Finally the γ branches on either side of this direction correspond to γ orbits, but are not symmetrical about it because they are very sensitive to rotations about the trigonal axis.

The minimum frequency for a direction 9.0° from the (0$\bar{1}$1) direction for τ is (1600 ± 10) T; this value compares favorably with the value of 1570 T obtained at the (0$\bar{1}$1) direction in the (1$\bar{1}$0) plane, since the frequency increases slightly as $\vec{H}$ is rotated from the (0$\bar{1}$1) direction in the (111) plane.

V. SUMMARY

The dHvA results of Brandt and Rayne[3] are extended and clarified, and three orbits (η, γ_2, and $\mu\gamma$) were observed for the first time by the dHvA effect. The dHvA frequencies and corresponding extremal cross-section areas for a variety of orbits are summarized in Table I. The minimum frequencies determined here for the β, τ, γ, and α orbits confirm the values of Brandt and Rayne[3] within the combined frequency and orientational accuracies. However, the value 3780 T for the α-orbit frequency with $\vec{H}$ along the (111) direction is considerably larger than the value 3450 T reported by Brandt and Rayne.[3] For measurements in the (1$\bar{1}$0) plane, the observed angular range of the η orbit is in good agreement with the range predicted by the four-plane-wave model of Bogle *et al.*,[7] whereas the sharp cutoff of the γ_2 orbit is consistent with the MAG V model of Dishman and Rayne.[6] These angular ranges indicate that the dimensions k_{LU}^{in} and k_{XU}^{in} for the hole surface are approximately 0.87 and 0.30 Å, respectively. For measurements in the (111) plane, the angular ranges of the τ, γ_2, and γ orbits show that

$$k_{TW}^{\text{in}} + k_{XK}^{\text{in}} \approx 0.40 \text{Å}^{-1}, \quad 0.866\, k_{XK}^{\text{out}} + k_{TU}^{\text{in}} \approx 0.47 \text{Å}^{-1},$$

and

$$0.866\, k_{XK}^{\text{out}} - k_{TU}^{\text{in}} < 0.18 \text{Å}^{-1},$$

respectively; so that

$$k_{XK}^{\text{out}} < 0.38 \text{ Å}^{-1}, \quad k_{TU}^{\text{in}} > 0.15 \text{ Å}^{-1},$$

and

$$k_{XK}^{\text{in}} < 0.25 \text{ Å}^{-1}.$$

In this way, the dHvA experiment provides information about inside and outside dimensions of the hole surface of mercury.

ACKNOWLEDGMENTS

We wish to thank C. Verge for excellent technical assistance. Research support from the National Research Council of Canada (NRC) and fellowships from NRC (to W. R. D. and R. G. P.) and the International Nickel Company of Canada (to R. G. P.) are gratefully acknowledged.

†Research supported by the National Research Council of Canada.

*International Nickel Company of Canada Predoctoral Fellow. Present address: University of Sussex, Brighton, England.

‡Present address: University of Waterloo, Waterloo, Ontario.

§E. W. R. Steacie Fellow of the National Research Council of Canada.

[1]B. I. Verkin, B. G. Lazarev, and W. S. Rudenko, Dokl. Akad. Nauk. SSSR 80, 45 (1951).

[2]D. Shoenberg, Phil. Trans. A245, 1 (1952).

[3]G. B. Brandt and J. A. Rayne, Phys. Rev. 148, 644 (1966).

[4]A. E. Dixon and W. R. Datars, Phys. Rev. 175, 928 (1968).

[5]W. R. Datars and A. E. Dixon, Phys. Rev. 154, 675 (1967).

[6]J. M. Dishman and J. A. Rayne, Phys. Rev. 166, 728 (1968).
[7]T. E. Bogle, J. B. Coon, and C. G. Grenier, Phys. Rev. 177, 1122 (1969).
[8]S. C. Keeton and T. L. Loucks, Phys. Rev. 152, 548 (1966).
[9]H. Jones, *The Theory of Brillouin Zones and Electronic States in Crystals* (North-Holland, Amsterdam, 1960), p. 58.
[10]J. Vanderkooy and W. R. Datars, Phys. Rev. 156, 671 (1967).
[11]R. W. Stark and L. R. Windmiller, Cryogenics 8, 272 (1968).
[12]A. Goldstein, S. J. Williamson, and S. Foner, Rev. Sci. Instr. 36, 1356 (1965).
[13]J. Vanderkooy, J. S. Moss, and W. R. Datars, J. Sci. Instr. 44, 949 (1967).
[14]R. A. Phillips and A. V. Gold, Phys. Rev. 178, 932 (1969).
[15]J. S. Moss and W. R. Datars, Phys. Letters A24, 630 (1967).
[16]R. G. Poulsen and W. R. Datars, Can. J. Phys. (to be published).

PHYSICAL REVIEW B VOLUME 3, NUMBER 10 15 MAY 1971

Determination of Relaxation Times by Magnetoacoustic Measurements in Copper†

Mee See Phua* and J. Roger Peverley
The Catholic University of America, Washington, D.C. 20017
(Received 19 August 1970)

Experimental and theoretical evidence is presented to support the hypothesis that the amplitudes of observable magnetoacoustic oscillations are to a large extent controlled by collision damping. By fitting experimental data on copper to a simple formula derived from the free-electron theory, we find that the temperature dependence of the electron-scattering rate for belly orbits is given by $(1.5 \pm 0.2) \times 10^6 T^3$ for temperatures below about 13 °K. This value is comparable to those obtained by other workers using cyclotron resonance. Although our method needs further theoretical development, we believe it has considerable potential as a tool for investigating scattering processes in metals.

I. INTRODUCTION

In a recent paper, Häussler and Welles[1] demonstrated that numerical values for the electron relaxation time in metals can be extracted from measurements on the amplitudes of Azbel'-Kaner cyclotron-resonance (AKCR) oscillations. The amplitude A_n of the nth resonance peak, is, according to free-electron theory, proportional to $n^2 e^{-2\pi n/\omega\tau}$, where ω is the microwave frequency and τ is the relaxation time. Since the cyclotron frequency ω_c is given by $\omega = n\omega_c$, this behavior has the simple physical interpretation that the amplitudes are primarily determined by the probability $e^{-2\pi/\omega_c\tau}$ that an electron can complete an orbit and return to the skin region where the microwave field is large. (This simple behavior is only followed when one can neglect the possibility that an electron completes more than one orbit, i.e., when $e^{-2\pi/\omega_c\tau} \ll 1$.) Häussler and Welles were able to obtain values for the effective scattering rate in copper as a function of temperature for several distinct orbits on the Fermi surface.

In this paper, we demonstrate that the magnetoacoustic analog of Häussler and Welles's experiment can be carried out. The magnetoacoustic effect involves spatial rather than temporal resonances, in fact resonance peaks occur whenever some suitable dimension on an electron orbit is a multiple of the sound wavelength. Several workers[2–4] have reported an exponential decrease of the amplitude of the observed oscillations with harmonic index n and we conclude that the regime $e^{-2\pi/\omega_c\tau} \ll 1$ is experimentally accessible.

II. THEORY

A. Free-Electron Model

Cohen, Harrison, and Harrison[5] have laid down the theoretical groundwork for a wide range of magnetoacoustic effects using the free-electron model and assuming an isotropic relaxation time τ (i.e., the electron mean free path is given by $l = v_F\tau$, where v_F is the Fermi velocity). They showed that for longitudinal sound waves of wave vector $\vec{q}$ in the presence of a transverse magnetic field $\vec{H}$ (normal to $\vec{q}$) the attenuation coefficient is given by

$$\alpha = \frac{Nm}{\rho v_s \tau} S_{11}(X, ql) , \tag{1}$$

where N is the electron density; m is the electron mass; ρ is the density of the metal; v_s is the sound velocity; and the argument X of the function S_{11} is given by $X = qR$, where R is the orbit radius, in real space, of an electron on an equatorial belt of